CRYSTAL GROWTH & DESIGN
2009
VOL. 9, NO. 8
3519–3524

Coordination-Induced Formation of One-Dimensional Nanostructures of Europium Benzene-1,3,5-tricarboxylate and Its Solid-State Thermal Transformation

Kai Liu,[†,‡] Hongpeng You,*[,†] Guang Jia,[†,‡] Yuhua Zheng,[†,‡] Yanhua Song,[†,‡] Mei Yang,[†,‡] Yeju Huang,[†,‡] and Hongjie Zhang*[,†]

State Key Laboratory of Rare Earth Resource Utilization, Changchun Institute of Applied Chemistry, Chinese Academy of Sciences, Changchun 130022, and Graduate School of the Chinese Academy of Sciences, Beijing 100049, P. R. China

Received March 1, 2009; Revised Manuscript Received May 15, 2009

ABSTRACT: Novel one-dimensional europium benzene-1,3,5-tricarboxylate compressed nanorods have been synthesized on a large scale through direct precipitation in solution phase under moderate conditions without the assistance of any surfactant, catalyst, or template. The obtained nanorods have widths of about 50−100 nm, thicknesses of 10−20 nm, and lengths ranging from a few hundred nanometers to several micrometers. X-ray powder diffraction, elemental analysis, Fourier transform infrared studies, and thermogravimetric and differential thermal analysis show that the nanorods have the structural formula of Eu(1,3,5-BTC)·$6H_2O$. Upon UV excitation, these nanorods exhibit a highly efficient luminescence, which comes from the Eu^{3+} ions. Moreover, Eu_2O_3 nanorods could also be obtained via a thermal decomposition method using the corresponding complex as a precursor. This synthetic route is promising for the preparation of other one-dimensional crystalline nanomaterials because of its simplicity and the low cost of the starting reagents.

Introduction

Physical and chemical properties of nanomaterials depend not only on their composition but also on their structure, morphology, phase, shape, size, distribution, and spatial arrangement.[1,2] Among the various nanostructures, one-dimensional (1D) nanoscaled materials, such as nanowires, nanorods, and nanotubes, have been regarded as significant factors that may influence the physical and chemical properties and bring wide applications.[3,4] Therefore, considerable attention has been paid to the strategies for fabricating 1D nanostructures including physical and chemical methods, such as laser-assisted catalysis growth,[5,6] vapor phase transport,[7,8] thermolysis,[9,10] and wet chemistry methods.[11−13]

Metal-organic frameworks that are based on metal ions coordinated by polydentate organic ligands have been developed extremely rapidly in recent years because of their potential application in catalysis,[14] gas storage,[15,16] sensors,[17] nonlinear optics,[18] and molecular recognition and separation.[19] However, these exploitations of their structures have generally been at the molecular level, and only a few are known about how their nano- or microscaled structures may be controlled and used[20−24] compared with inorganic materials.

Rare earth organic coordination compounds have been extensively utilized in high-performance luminescent devices, magnets, catalysts, and other functional materials because of their electronic, optical, and chemical characteristics resulting from the 4f electronic shells.[25,26] Among them, the Eu^{3+} compounds is one of the most important luminescent materials, which have been regarded as attractive because of their strong red emissions. Polycarboxylate anions with aromatic rings are widely used in the construction of high-dimensional lanthanide coordination complexes because these anions are able to act as bridging ligands in various ligating modes.[27] Recently, Chen et al. have reported the preparation of microporous metal-organic framework based on Eu^{3+} and 1,3,5-BTC, which makes use of luminescent open Eu^{3+} sites for the sensing of small molecules.[28] To date, a great number of works have dealt with 1D nanostructured rare earth inorganic materials,[29] which can be designed as functional nanodevices because of their electrical or luminescent behaviors. However, fewer studies have been performed on rare earth organic coordination complexes,[30] although they have high fluorescence efficiencies, narrow emission bands, and excellent fluorescence monochromaticity, and can be applied in a variety of areas such as light conversion materials, organic electroluminescent devices, optical microcavity emitters, etc.[31,32]

In the present paper, we present the first preparation of well-dispersed metal-organic framework (Europium benzene-1,3,5-tricarboxylate) nanorods via direct precipitation in solution phase in needless of high pressure or temperature. A plausible mechanism responsible for the formation of nanorods is also given. And the optical properties were investigated in detail. Furthermore, rodlike Eu_2O_3 was obtained through high-temperature calcination of Eu(1,3,5-BTC)·$6H_2O$.

Experimental Section

Materials. The initial chemicals, including Eu_2O_3 (99.99%, Changchun Applied Chemistry Science and Technology Limited, China), benzene-1,3,5-tricarboxylic acid(1,3,5-BTC) (98%, Alfa Aescar Chemical Co.), HNO_3, and ethanol (all with purity of A. R., Beijing Fine Chemical Company, China), were used without further purification.

Preparation. $Eu(NO_3)_3$ aqueous solution were obtained by dissolving Eu_2O_3 (99.99%) in dilute HNO_3 solution under heating with agitation. In a typical experiment, 1 mmol of $Eu(NO_3)_3$ aqueous solution was introduced into 10 mL of ethanol first, and the solution was added into 1 mmol of 1,3,5-BTC ethanol−water solution (30 mL, v/v = 1:1) under vigorous stirring at room temperature. The reaction mixture was then refluxed at 90 °C under constant stirring for 2 h, and a large amount of white precipitate occurred. At last, the precipitate was collected by centrifugation, washed several times with ethanol and water, and dried at 60 °C for 24 h in atmosphere.

To investigate the effect of reaction time on the morphology, we also refluxed the reaction mixture at 90 °C for 4 and 6 h, respectively,

* To whom correspondence should be addressed. Email: hpyou@ciac.jl.cn or hongjie@ciac.jl.cn.
† State Key Laboratory of Rare Earth Resource Utilization.
‡ Graduate School of the Chinese Academy of Sciences.

10.1021/cg900252r CCC: $40.75
Published on Web 06/15/2009

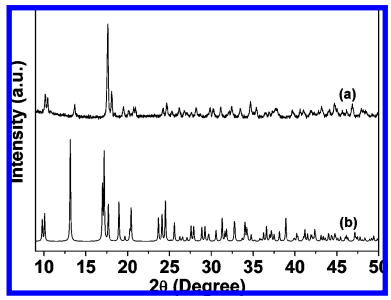

Figure 1. (a) XRD pattern of the as-obtained Eu(1,3,5-BTC)·$6H_2O$ and (b) simulated XRD pattern using the X-ray structure of La(1,3,5-BTC)·$6H_2O$ single crystal.

with the other conditions held fixed. In addition, the conversion of Eu(1,3,5-BTC)·$6H_2O$ into Eu_2O_3 was carried out in an oven at 600 °C for 2 h in air.

Characterization. Elemental analysis of C, H, and Eu in the solid samples were carried out on VarioEL (Elementar Analysensysteme GmbH) and inductive coupled plasma (ICP) atomic emission spectrometric analysis (POEMS, TJA), respectively. Powder X-ray diffraction (XRD) patterns were performed on a D8 Focus (Bruker) diffractometer (continuous, 40 kV, 40 mA, increment = 0.02°). Fourier transform infrared spectroscopy (FT-IR) spectra were measured with a Perkin-Elmer 580B infrared spectrophotometer with the KBr pellet technique. Thermogravimetric analysis and differential thermal analysis (TGA-DTA) data were recorded with a thermal analysis instrument (SDT2960, TA Instruments, New Castle, DE) at the heating rate of 10 °C min^{-1} in an air flow of 100 mL min^{-1}. The morphology and composition of the samples were inspected using a field emission scanning electron microscope (FE-SEM, S-4800, Hitachi) equipped with an energy-dispersive X-ray spectrum (EDX, JEOL JXA-840). Transmission electron microscopy (TEM) images were obtained using a JEOL 2010 transmission electron microscope operating at 200 kV. Photoluminescence (PL) excitation and emission spectra were recorded with a Hitachi F-4500 spectrophotometer equipped with a 150 W xenon lamp as the excitation source. The luminescence decay curves were obtained from a Lecroy Wave Runner 6100 Digital Osilloscope (1GHZ) using a tunable laser (pulse width = 4 ns, gate = 50 ns) as the excitation (Continuum Sunlite OPO). All the measurements were performed at room temperature.

Results and Discussion

Elemental analysis was used to investigate the composition of the as-obtained products. The experimental contents of C, H, and Eu are shown to be 23.40, 3.29, and 32.37%, respectively, which are basically in agreement with theoretical value of C (23.14%), H (3.24%) and Eu (32.53%), confirming the molecular formula Eu(1,3,5-BTC)·$6H_2O$.

Figure 1a shows powder X-ray diffraction pattern of the final products. It can be seen that the sample of Eu(1,3,5-BTC)·$6H_2O$ was crystalline in spite of the moderate reaction conditions. All the diffraction peaks can be well-indexed to a known bulk phase of La(1,3,5-BTC)·$6H_2O$ (Figure 1b)[33] except for a spectral shift toward the larger angle side, revealing that the as-obtained sample is isostructural with the La(1,3,5-BTC)·$6H_2O$ structure. The spectral shift of the diffraction peaks can be explained by the change of ionic radii. When the La^{3+} ion was substituted by the Eu^{3+} ion with a smaller radius as a result of lanthanide contraction, the crystal lattice constants as well as *d*-spacing decreased, and thus the diffraction angles increased accordingly because of the Bragg equation $2d \sin \theta = \lambda$, where *d* is the distance between two crystal planes, θ is diffraction angle of an observed peak, and λ is the X-ray wavelength (0.15405 nm). On the basis of the crystal structure of the bulk phase La(1,3,5-BTC)·$6H_2O$,[33] the crystal structure of the Eu(1,3,5-BTC)·$6H_2O$ can thus be monoclinic, space group *Cc*. The symmetric unit

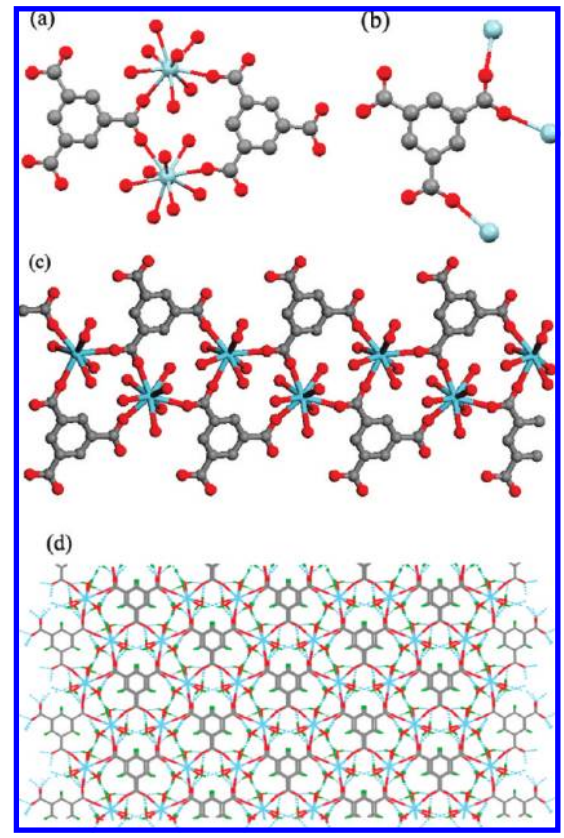

Figure 2. (a) Symmetric unit. (b) Coordination modes of the carboxylate groups. (c) 1D ribbonlike structure along the *a* axis. (d) Perspective view of the packing along the *c* axis of the Eu(1,3,5-BTC)·$6H_2O$. All the figures were drawn using the CIF file of isostructural La(1,3,5-BTC)·$6H_2O$. The hydrogen atoms were omitted for clarity in a−c. Dotted lines symbolize hydrogen bonds. Eu blue, O red, C gray, H green.

of the product is shown in Figure 2a. The center Eu atom is nine-coordinated by six oxygen atoms from water molecules as well as three oxygen atoms from three carboxylate groups of 1,3,5-H_3BTC ligands to form a tricapped trigonal prismatic geometry. Three carboxylate groups of the ligand represent different coordination modes (Figure 2b). One bonding carboxylate group is unidentate, one is bidentate, and each ligand also presents a free carboxylate group. As shown in Figure 2c, the structure consists of parallel 1D ribbonlike molecular motifs extending along the *a* axis. These 1D molecular motifs are further stacked in such a way that phenyl groups of the 1,3,5-H_3BTC ligands superimpose along the *c* axis. In addition, the combination of noncovalent interactions (hydrogen-bonding and $\pi-\pi$ stacking) leads to the formation of a 3D network structure (Figure 2d).

The FTIR spectra also allows insights into the chemical composition of europium benzene-1,3,5-tricarboxylate. In Figure 3, the characteristic bands of the nonionized carboxyl group of 1,3,5-BTC disappear (ν_{-OH}, 3087 cm^{-1}; $\nu_{C=O}$, 1721 cm^{-1}; $\delta_{C=O}$, 531 cm^{-1}) and new bands appear in the regions 1614−1558, 1436−1374 cm^{-1}, and 535 cm^{-1} which belong to the stretching vibrations $\nu_{as}(-COO^-)$ and $\nu_s(-COO^-)$ of the carboxylate ions, and the Eu−O stretching vibration, respectively.[34] These new bands prove that the Eu^{3+} ions have been coordinated with the 1,3,5-BTC ligands successfully.[34] Besides, the bands $\nu(-OH)$ in the FTIR spectra (Figure 3b), which lie in the region of 3409 cm^{-1}, indicate that water molecules act as not only the solvent

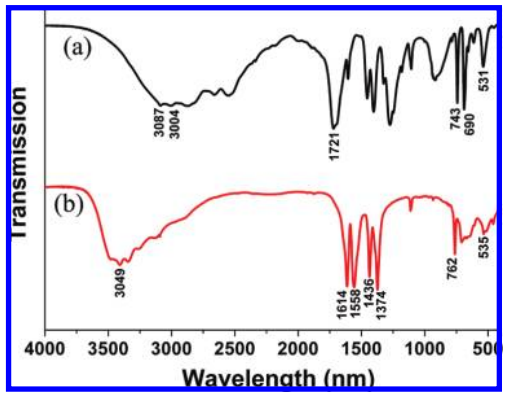

Figure 3. FT-IR spectra of samples (a) 1,3,5-H_3BTC and (b) Eu(1,3,5-BTC)·$6H_2O$.

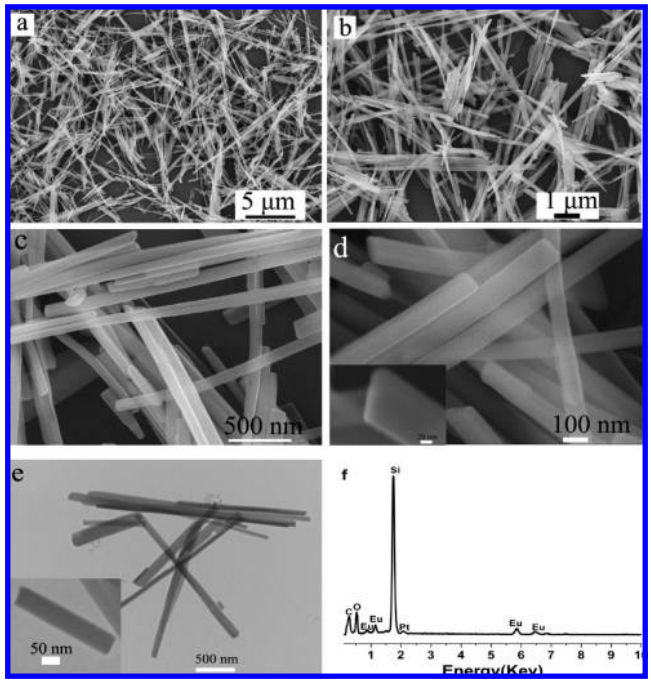

Figure 4. (a−d) FE-SEM images, (e) TEM images, and (f) the EDX spectrum (the Pt and Si peaks arising from measurement) of Eu(1,3,5-BTC)·$6H_2O$.

but also the reactant for the europium benzene-1,3,5-tricarboxylate formation.[34b]

The thermal behaviors of the as-synthesized products were investigated with TG-DTA measurements (see Figure S1 in the Supporting Information). There are two major stages of rapid weight loss in the TGA curve at about 109.89 and 468.76 °C, accompanying their corresponding endothermic and exothermic peaks. It indicates that the samples may decompose to produce Eu_2O_3 by the two steps. The weight loss for the first and second stages were measured to be 22.53 and 41.97%, which are basically in agreement with the theoretical value of assumed structure Eu(1,3,5-BTC)·$6H_2O$ to loss the six water molecules (23.14%) and organic ligand (39.19%), respectively.

The size and morphology of the Eu(1,3,5-BTC)·$6H_2O$ nanorods were examined by field emission scanning electron microscopy (FE-SEM) and transmission electron microscopy (TEM). Figure 4 shows typical images of the products (1:1, 90 °C, 2 h) at different magnifications. One can notice that the rodlike structures dominate in the full images (Figure 4a,b),

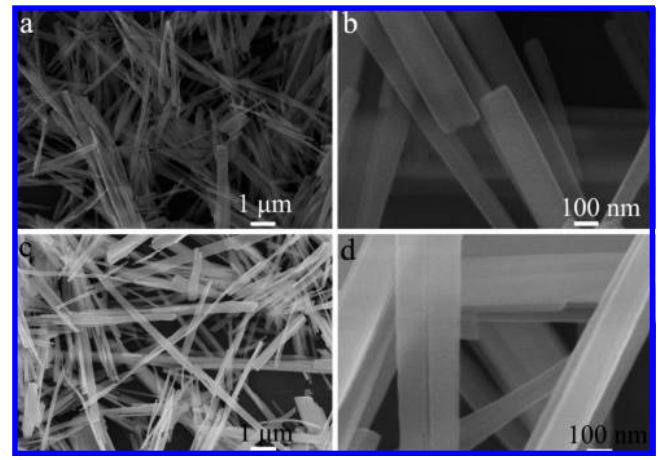

Figure 5. FE-SEM images of the Eu(1,3,5-BTC)·$6H_2O$ at different magnifications ((a, b) for 1:1, 90 °C, 4 h; (c, d) for 1:1, 90 °C, 6 h).

indicating a high yield of our products. Closer observations (Figure 4c,d) show the detailed structures of these rodlike morphologies, indicating that all of the nanorods are compressed and well-separated from each other, which have widths of about 50−100 nm, thicknesses of 10−20 nm, and lengths ranging from a few hundred nanometers to several micrometers. Figure 4f shows the EDX spectrum of the final product, which confirmed that no elements other than C, O, and Eu present except the Si and Pt peaks from measurement. The results are in agreement with the elemental analysis.

TEM analysis provides further insight into the morphology and microstructure details of the Eu(1,3,5-BTC)·$6H_2O$ nanorods. Figure 4e shows a typical TEM image of as-prepared products, clearly showing that the sample is entirely composed of relatively uniform nanorods, which is consistent with the results shown in the SEM images (Figure 4a−d). A typical high-magnification TEM image of a single nanorod (inset in Figure 4e) indicates that the resulting nanorods have electron-microscopically perfectly smooth surface. TEM investigation also reveals that the Eu(1,3,5-BTC)·$6H_2O$ nanorods are homogeneous.

We investigated the influence of reaction time on the morphology of the Eu(1,3,5-BTC)·$6H_2O$. Figure 5 gives the products obtained at different reaction time. One can clearly see that reaction time played an important role in determining the morphology of the Eu(1,3,5-BTC)·$6H_2O$. When reaction time was extended to 4 h for the reflux process, the product showed rodlike morphology which was still similar to the as-obtained sample (1:1, 90 °C, 2 h) in size (Figure 5a,b). A further detailed observation reveals that these compressed nanorods still have a good dispersity (Figure 5b). However, when the reaction time increased to 6 h, the product mainly contained a large quantity of aggregated nanorods (Figure 5c,d) with the widths of 100−200 nm, thicknesses of 50−100 nm, and lengths of several micrometers. Therefore, we can conclude that appropriate reaction time was necessary for the synthesis of these well-dispersed rodlike nanostructures in our experiments.

Up to now, a great number of 1D nanostructures have been reported.[3−13] Those reports have revealed that the formation of the final products may depend on the two factors: the inner and external forces. The inner forces mainly include the growth habits of crystal and the phase structure of the sample, whereas crystal-face attraction, electrostatic and dipolar fields associated with the aggregate, van der Waals forces, hydrophilic or hydrophobic interaction, and hydrogen bonds belong to the

Scheme 1. Structural Schematic Diagram on Formation Process of the Eu(1,3,5-BTC)·6H$_2$O Compressed Nanorods (Hydrogen Atoms Omitted for Clarity; Eu Blue, O Red, C Gray)

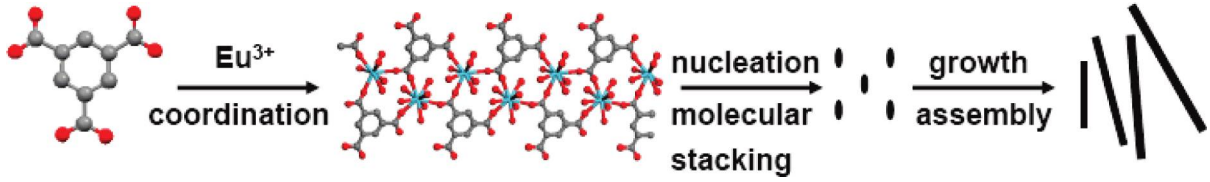

external forces. All of them have various effects on the formation of 1D nanostructures. Although the exact mechanism for the formation of these rodlike nanostructures in our experiments is still unclear, we believe that the inner and external forces are key factors in the process. Coordination-induced self-assembling Eu(1,3,5-BTC)·6H$_2$O molecules into one-dimensional structures represents a balance between the inner force of molecular stacking and the external force of solubility.

On one hand, the crystal structure of the Eu(1,3,5-BTC)·6H$_2$O discussed above exhibits parallel 1D ribbonlike structure by coordination interaction. As depicted in Figure 2c, the 1,3,5-BTC ligands bridge adjacent the Eu^{3+} ions to form 1D ribbonlike molecular motifs extending along the *a* axis. The occurrence of 1D ribbon in the compound is attributable to the steric orientation of the carboxylate groups of 1,3,5-BTC. This observation suggests that the flexible coordination mode of the 1,3,5-BTC ligand in combination with the high coordination number of the Eu^{3+} ions favors the formation of 1D ribbonlike structure. Therefore, the possible process from coordination-induced molecular stacking to formation the 1D nanostructures can be briefly presented as following: when Eu^{3+} and 1,3,5-BTC are mixed together, the oxygen atoms on the $-COO^-$ of 1,3,5-BTC aromatic ring can coordinate to Eu^{3+} ions, resulting in 1,3,5-BTC-bridged structure. The Eu species contained in the as-formed structure can then further capture other 1,3,5-BTC molecules by coordination interactions along the same direction. Finally, this coordination-induced assembly process can proceed repeatedly until the depletion of reactants in the solution, resulting in the formation of well-dispersed nanorods. Additionally, the organic ligand of 1,3,5-H$_3$BTC may have the function as the potential crystal face inhibitor in the formation process of nanorods except acting as the reactant, which benefits the formation of oriented nucleation and leads to the construction of anisotropic growth of the nanorods.

On the other hand, the polar solvent plays an important role in the anisotropic growth process. A sufficient solubility is crucial for the ligand 1,3,5-BTC molecule, which can react with the Eu species in the mixed water and ethanol solvents. The final product Eu(1,3,5-BTC)·6H$_2$O becomes insoluble in the polar solvents where the molecule has minimum interaction with the solvents, which benefits for the 1D self-assembly through molecular stacking interaction.

Therefore, we can suggest that the formation of 1D nanostructures in our present study is attributed to coordination-induced assembly from the Eu^{3+} ions and 1,3,5-BTC in polar solvent.[23,24,35,36] The structural schematic diagram on formation process of the Eu(1,3,5-BTC)·6H$_2$O compressed nanorods is summarized in Scheme 1.

All the Eu(1,3,5-BTC)·6H$_2$O samples prepared under different conditions exhibit similar photoluminescence properties. The strong red light emission of the nanorods solution upon excitation at 254 nm with a UV lamp can be seen clearly (inset in Figure 6b). The excitation spectrum (Figure 6a) was obtained by monitoring the emission of the $^5D_0-^7F_2$ transition of the Eu^{3+} ions at 615 nm. It can be seen clearly that the excitation spectrum consists of a broadband and some weak lines in the range from 350 to 500 nm. The broadband with two maximum at 260 and 292 nm are due to the charge-transfer band between the O^{2-} and Eu^{3+} ions and $\pi-\pi^*$ electron transition of the organic bridging ligand, respctively.[37] The weak lines at 364, 384, 397, 418, and 467 nm are contributed to the $^7F_0-^5D_4$, $^7F_0-^5G_J$, $^7F_0-^5L_6$, $^7F_0-^5D_3$, and $^7F_0-^5D_2$ transitions, respectively. Figure 6b illustrates the emission spectrum excited at 260 nm. The peaks at about 533, 576, 589, 615, 649, and 698 nm are assigned to the $^5D_1-^7F_1$ and $^5D_0-^7F_J$ ($J = 0, 1, 2, 3, 4$) transitions of the Eu^{3+} ions, respectively. The $^5D_0-^7F_0$ transition appears since the Eu^{3+} ions in the Eu(1,3,5-BTC)·6H$_2$O nanorods occupy sites with a low symmetry because Eu(1,3,5-BTC)·6H$_2$O belongs to monoclinic space group *Cc*. The $^5D_0-^7F_1$ transition for the rodlike Eu(1,3,5-BTC)·6H$_2$O corresponds to a magnetic dipole transition, and the intensity of this emission is medium-strong. The most intense emission in the luminescent spectra is the $^5D_0-^7F_2$ transition at 615 nm for the Eu(1,3,5-BTC)·6H$_2$O nanorods, which is the so-called hypersensitive transition and is responsible for the brilliant-red emission of these products. The $^5D_0-^7F_3$ and $^5D_0-^7F_4$ transitions at 649 nm and 698 nm, are all nearly invisible for the Eu(1,3,5-BTC)·6H$_2$O nanorods.

The kinetic properties for the luminescence of the Eu(1,3,5-BTC)·6H$_2$O nanorods were investigated by PL decay curve (see

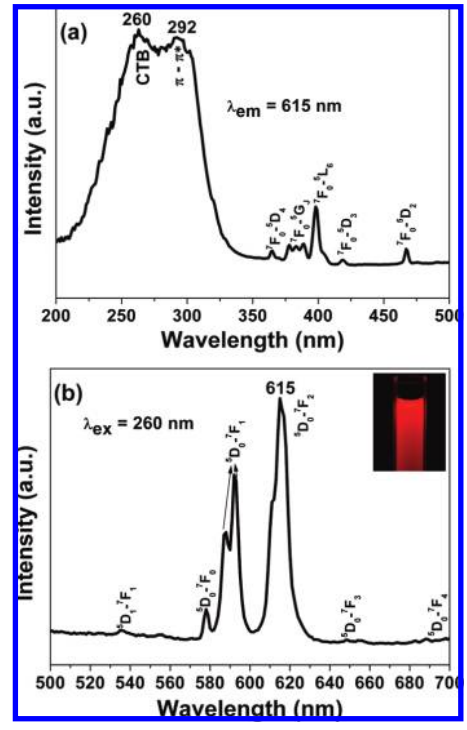

Figure 6. (a) PL excitation spectra of Eu(1,3,5-BTC)·6H$_2$O monitored at 615 nm; (b) PL emission spectra of Eu(1,3,5-BTC)·6H$_2$O under excitation at 260 nm; the inset shows the corresponding luminescence photograph of the sample dispersed in the ethanol solution.

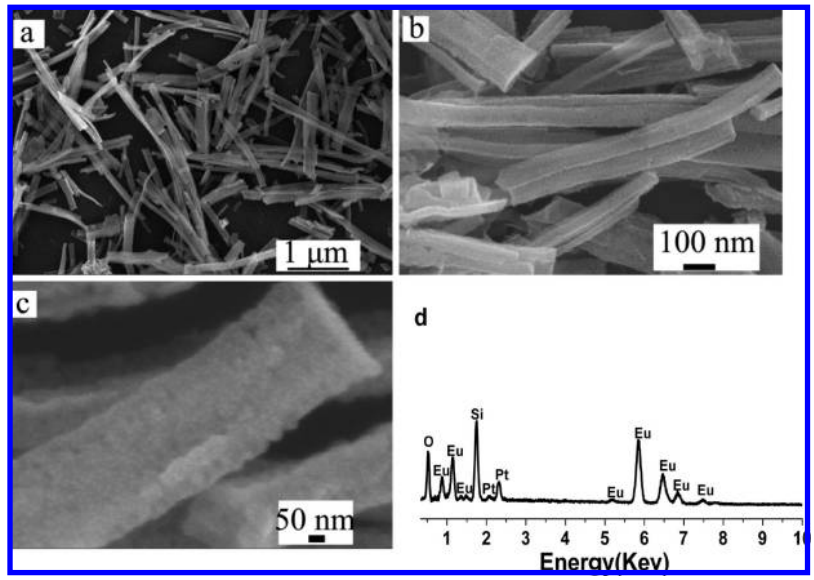

Figure 7. (a−c) FE-SEM images of the Eu_2O_3 sample and (d) EDX spectrum of the Eu_2O_3 (The Pt and Si peaks arising from measurement).

Figure S2 in the Supporting Information). The decay curve for the luminescence of the Eu^{3+} ions was monitored by the $^5D_0-^7F_2$ transition (615 nm). It is well fitted into a single-exponential function as $I = I_0 \exp(-t/\tau)$, where I and I_0 are the luminescence intensities at times t and 0, respectively, and τ is defined as the luminescence lifetime. The lifetime of the Eu^{3+} ions is determined to be 0.19 ms, which can be comparable with Eu^{3+}-doped inorganic luminescent materials.[38]

The as-synthesized rare earth complex nanorods should provide a useful source for 1D rare earth oxide materials, as the europium ions are distributed uniformly in the Eu(1,3,5-BTC)·$6H_2O$ nanorods. As is shown in Figure 3a, weight loss in the second step in TGA curve between 400 and 500 °C was ascribed to [Eu(1,3,5-BTC) → $Eu_2O_3 + H_2O + CO_2$], which is discussed above. Therefore, the Eu_2O_3 nanostructure can be obtained by calcination of the as-made Eu(1,3,5-BTC)·$6H_2O$. Anneal treatment at 600 °C in air for 2 h resulted in a white powder of Eu_2O_3. The XRD pattern (see Figure S3 in the Supporting Information) shows that all of the peaks can be well-indexed to the pure cubic face-centered phase of Eu_2O_3 (JCPDS 32−0380), indicating that the pure phase of Eu_2O_3 can be obtained by annealing the Eu(1,3,5-BTC)·$6H_2O$ precursors directly. In addition, the broadened width of these peaks indicates the nanosized nature of the products, in accordance with the SEM results.

Figure 7 gives the morphologies of the Eu_2O_3 samples. One can notice that the as-grown rodlike crystal is maintained in great part during the solid-state transformation with diameters of 80−100 nm and lengths of 1−2 μm. Meanwhile, size shrinkage and aggregation of nanorods occurred during the heating process because of the dehydration and decarboxylation of the Eu(1,3,5-BTC)·$6H_2O$. Furthermore, one can see clearly from the SEM image (Figure 7c) that the surface of the as-obtained Eu_2O_3 are actually rough, which may be ascribed to the release of the CO_2 gas generated in the process of decarboxylation process. Additionally, energy dispersive X-ray spectrum was further used to investigate the as-obtained Eu_2O_3 samples. It can be seen from Figure 7d that the final products after calcinations at 600 °C are composed of the two elements (Eu and O), indicating that the as-obtained precursor has almost decomposed completely and converted to crystalline Eu_2O_3 during the annealing process. This is consistent with the XRD results of the calcined samples.

The luminescence properties of the Eu_2O_3 nanorods were also investigated. The excitation spectrum (see Figure S4 in the Supporting Information) consists of a broadband (260 nm) and some peaks in the range from 350 to 500 nm, which can be assigned to the charge-transfer band of the Eu−O and the f−f transitions of the Eu^{3+} ions. The emission spectrum exhibits the strongest emission peak at 610 nm. This result is similar to those of the Eu_2O_3 nanoparticles, nanorods, and nanotubes.[39]

Conclusions

In summary, we have successfully developed an effective and facile method for self-assembling europium benzene-1,3,5-tricarboxylate molecules into compressed nanorods. To our knowledge, this is the first time that europium benzene-1,3,5-tricarboxylate nanorods have been prepared. The as-prepared samples show a strong red emission under ultraviolet excitation, and the lifetime is also determined. Interestingly, the nanoscaled metal-organic compound turns into shape-preserved Eu_2O_3 when heated in air. The retention of rodlike morphology of the as-grown crystals during the solid-state transformation suggests a potential approach for fabricating 1D inorganic nanomaterials from metal-organic precursors. Moreover, this general, simple, green, and high-yield strategy described here may serve as a guidance for the design and fabrication of novel nanodevices in photochemical, electrochemical, and biochemical fields.

Acknowledgment. This work is financially supported by the National Natural Science Foundation of China (Grant 20771098.) and the National Basic Research Program of China (973 Program, Grants 2007CB935502 and 2006CB601103).

Supporting Information Available: Additional figures (PDF). This material is available free of charge via the Internet at http://pubs.acs.org.

References

(1) El-Sayed, M. A. *Acc. Chem. Res.* **2001**, *34*, 257.
(2) Wang, Z. L.; Song, J. H. *Science.* **2006**, *312*, 242.

(3) Goldberger, J.; Fan, R.; Yang, P. D. *Acc. Chem. Res.* **2006**, *39*, 239.
(4) Lin, Y. R.; Yang, S. S.; Tsai, S. Y.; Hsu, H. C.; Wu, S. T.; Chen, I. *Cryst. Growth Des.* **2006**, *6*, 1951.
(5) Duan, X. F.; Lieber, C. M. *Adv. Mater.* **2000**, *12*, 298.
(6) Morales, A. M.; Lieber, C. M. *Science.* **1998**, *279*, 208.
(7) Wang, Z. Q.; Liu, X. D.; Gong, J. F.; Huang, H. B.; Gu, S. L.; Yang, S. G. *Cryst. Growth Des.* **2008**, *8*, 3911.
(8) Huang, M. H.; Wu, Y. Y.; Feick, H.; Tran, N.; Weber, E.; Yang, P. D. *Adv. Mater.* **2001**, *13*, 113.
(9) Jun, Y. W.; Choi, C. S.; Cheon, J. *Chem. Commun.* **2001**, 101.
(10) Deng, Z. X.; Wang, C.; Sun, X. M.; Li, Y. D. *Inorg. Chem.* **2002**, *41*, 869.
(11) Warner, J. H. *Adv. Mater.* **2008**, *20*, 784.
(12) Zhang, H.; Wang, D. Y.; Yang, B.; Helmuth, M. *J. Am. Chem. Soc.* **2006**, *128*, 10171.
(13) Yu, Y. T.; Qiu, H. B.; Wu, X. W.; Li, H. C.; Chen, S. N. *Adv. Funct. Mater.* **2008**, *18*, 541.
(14) Xing, B.; Choi, M. F.; Xu, B. *Chem.—Eur. J.* **2002**, *8*, 5028.
(15) Maji, T. K.; Matsuda, R.; Kitagawa, S. *Nat. Mater.* **2007**, *6*, 142.
(16) Mulfort, K. L.; Hupp, J. T. *J. Am. Chem. Soc.* **2007**, *129*, 9604.
(17) (a) Beck, J. B.; Rowan, S. J. *J. Am. Chem. Soc.* **2003**, *125*, 13922. (b) Meng, Q. G.; Boutinaud, P.; Zhang, H. J.; Mahiou, R. *J. Lumin.* **2007**, *124*, 15.
(18) Selvakumar, S.; Ravi Kumar, S. M.; Rajarajan, K.; Joseph Arul Pragasam, A.; Rajasekar, S. A.; Thamizharasan, K.; Sagayaraj, P. *Cryst. Growth Des.* **2006**, *6*, 2607.
(19) Kosal, M. E.; Chou, J. H.; Wilson, S. R.; Suslick, K. S. *Nat. Mater.* **2002**, *1*, 118.
(20) Moonhyun, O.; Chad, A, M. *Nature* **2005**, *438*, 651.
(21) You, M. J.; Jungseok, H.; Chad, A, M. *J. Am. Chem. Soc.* **2007**, *129*, 7480.
(22) Yan, B.; Qiao, X. F. *J. Phys. Chem. B* **2007**, *111*, 12362.
(23) Hu, J. S.; Guo, Y. G.; Liang, H. P.; Wan, L. J.; Jiang, L. *J. Am. Chem. Soc.* **2005**, *127*, 17090.
(24) Sun, X. P.; Dong, S. J.; Wang, E. K. *J. Am. Chem. Soc.* **2005**, *127*, 13102.
(25) (a) Buunzli, G. J. C.; Piguet, C. *Chem. Rev.* **2002**, *102*, 1897. (b) Tsukube, H.; Shinoda, S. *Chem. Rev.* **2002**, *102*, 2389. (c) Capecchi, S.; Renault, O.; Moon, D. G.; Halim, M.; Etchells, M.; Dobson, P. J.; Salata, O. V.; Christou, V. *Adv. Mater.* **2000**, *12*, 1591.
(26) (a) Ananias, D.; Ferdov, S.; Almeida Paz, F.; Sá Ferreira, R.; Ferreira, A.; Geraldes, F.; Carlos, L.; Lin, Z.; Rocha, J. *Chem. Mater.* **2008**, *20*, 205(b) Kido, J.; Okamoto, Y. *Chem. Rev.* **2002**, *102*, 2357.
(27) (a) Wang, Z.; Kravtsov, V. C.; Zaworotko, M. J. *Angew. Chem., Int. Ed.* **2005**, *44*, 2877. (b) Rosi, N. L.; Kim, J.; Eddaoudi, M.; Chen, B.; O'Keeffe, M.; Yaghi, O. M. *J. Am. Chem. Soc.* **2005**, *127*, 1504.
(28) Chen, B. L.; Yang, Y.; Zapata, F.; Lin, G. N.; Qian, G. D; Lobkovsky, E. B. *Adv. Mater.* **2007**, *19*, 1693.
(29) (a) Xu, A. W.; Fang, Y. P.; You, L. P.; Liu, H. Q. *J. Am. Chem. Soc.* **2003**, *125*, 1494. (b) Li, X.; Li, Q.; Xia, Z. G.; Wang, L.; Yan, W. X.; Wang, J. Y.; Boughton, R. I. *Cryst. Growth Des.* **2006**, *6*, 2193.
(30) William, J. R.; Kathryn, M. L.; An, H. Y.; Lin, W. L.; Lin, W. B. *J. Am. Chem. Soc.* **2006**, *128*, 9024.
(31) Hong, Z. *Adv. Mater.* **2001**, *13*, 1241.
(32) Kuriki, K.; Kolike, Y. *Chem. Rev.* **2002**, *102*, 2347.
(33) Wen, Y. H.; Cheng, J. K.; Feng, Y. L.; Zhang, J.; Li, Z. J.; Yao, Y. G. *Chinese J. Struct. Chem.* **2005**, *12*, 1440.
(34) (a) Zhao, G. H.; Gao, J. Z.; Zhao, J.; Teng, X. L.; Kang, J. W. *Synth. React. Inorg. Met-Org. Chem.* **1998**, *28*, 1405. (b) Yang, J.; Yue, Q.; Li, G. D.; Cao, J. J.; Li, G. H.; Chen, J. S. *Inorg. Chem.* **2006**, *45*, 2857.
(35) Kaushik, B.; Aniket, D.; Randy, O.; Chen, H.; Zuo, J. M.; Zang, L. *J. Am. Chem. Soc.* **2005**, *127*, 10496.
(36) Cui, F.; Zhang, J. H.; Cui, T. Y.; Liang, S.; Ming, L.; Gao, Z. M.; Yang, B. *Nanotechnology* **2008**, *19*, 065607.
(37) Yang, Y. S.; Gong, M. L.; Li, Y. Y. *J. Alloys Compd.* **1994**, *207—208*, 112.
(38) (a) Jia, G.; Yang, M.; Song, Y. H; You, H. P.; Zhang, H. J. *Cryst. Growth Des.* **2009**, *9*, 301. (b) Jia, G.; Zheng, Y. H.; Liu, K.; Song, Y. H.; You, H. P.; Zhang, H. J *J. Phys. Chem. C* **2009**, *113*, 153.
(39) (a) Wakefield, G.; Keron, H. A.; Dobson, P. J.; Hutchison, J. L. *J. Colloid Interface Sci.* **1999**, *215*, 179. (b) Panda, A. B.; Glaspell, G.; El-Shall, M. S. *J. Phys. Chem. C* **2007**, *111*, 1861. (c) Wu, G.; Zhang, Li.; Cheng, B.; Xie, T.; Yuan, X. *J. Am. Chem. Soc.* **2004**, *126*, 5976.

CG900252R